Silicon (2018) 10:759–767
DOI 10.1007/s12633-016-9527-4

ORIGINAL PAPER

Reduction in Photocurrent Loss and Improvement in Performance of Single Junction Solar Cell Due to Multistep Grading of Hydrogenated Amorphous Silicon Germanium Active Layer

Duy Phong Pham[1] · **Sangho Kim**[2] · **Jinjoo Park**[1] · **Anh Huy Tuan Le**[1] · **Jaehyun Cho**[2] · **Junhee Jung**[2] · **S. M. Iftiquar**[1] · **Junsin Yi**[1]

Received: 11 August 2016 / Accepted: 10 November 2016 / Published online: 12 April 2017

Abstract Single junction solar cells were fabricated with intrinsic hydrogenated amorphous silicon germanium (a-SiGe:H) as the active layer, that shows a 10% photovoltaic conversion efficiency. The a-SiGe:H active layer of the solar cells of type-A had constant band gap materials while that of type-B had a four step graded band gap by composition gradient (CG). The cells with composition gradient show an enhancement in fill factor and open circuit voltage (V_{oc}) by 5% and 20 mV respectively, with respect to a cell without the graded band gap active layer. Such an enhanced device performance is attributed to reduction in recombination loss of photo-generated electron hole pairs. The effect of this photo-current loss was investigated in the electrical bias dependent external quantum efficiencies (EQE), illumination dependent current-voltage measurements and dark current-voltage characteristics. The device parameters like reverse saturation current density (J_o), series resistance (R_s) and diode quality factor (n) were also estimated. In comparison to the cell without the composition gradient, the EQE shows a reduced recombination loss across the whole wavelength range for the cell with the CG. Furthermore, the introduction of the CG results in a significantly increased shunt resistance from 720 to 1200 Ω.cm^2. The estimated n values of the cells under dark operating condition, decreases from 1.8 to 1.7 along with J_o from 3×10^{-7} down to 4.5×10^{-8} A/cm^2 with CG, while the same parameters decreased from 3.73 to 3.06, 2.96×10^{-6} to 3.05×10^{-7} A/cm^2 respectively under AM1.5G insolation.

Keywords Amorphous silicon solar cell · Amorphous silicon germanium · Composition gradient process · Carrier recombination

1 Introduction

The hydrogenated amorphous silicon solar cell is known to be one of the promising photovoltaic devices for generating electrical energy from sunlight. Extensive research has been going on to improve performance of the device so that it becomes a commercially viable product. Its low efficiency is one of the primary limiting factors that needs to be improved. In a multi-junction cell structure, the initial efficiency of 16.3% was reported in 2011 for the triple junction solar cells (a-Si:H/a-SiGe:H/μc-Si:H) [1], yet it seems that the technology should improve further for large scale commercialization. High efficiency single junction solar cells can be integrated into a multi-junction architecture. Therefore, efficiency improvement of a single junction solar cell is certainly one of the fundamental requirements. Hydrogenated amorphous silicon germanium (a-SiGe:H) can be used in a low band gap sub-cell [2, 3]. Such a low band gap device is thought to suffer from higher electronic defects of an a-SiGe:H intrinsic or active layer such as dangling bonds, vacancies, microvoids and Urbach tail defects [4–6] etc. One of the advantages of the a-SiGe:H based solar cell is that it may show higher short-circuit current density (J_{sc}) with reference to a solar cell with a hydrogenated

✉ S. M. Iftiquar
iftiquar@skku.edu

✉ Junsin Yi
yi@yurim.skku.ac.kr

1 College of Information and Communication Engineering, Sungkyunkwan University, Suwon 440-746, Republic of Korea

2 Department of Energy Science, Sungkyunkwan University, Suwon 440-746, Republic of Korea

amorphous silicon (a-Si:H) active layer [7]. A high J_{sc} of the a-SiGe:H top or middle cell is necessary for raising the matched current in a high efficiency multi-junction thin film solar cell structure [7]. However, lowering of band-gap of the i-layer by an increase in Ge content within the film may be accompanied by a detrimental open-circuit voltage (V_{oc}) and fill factor (FF) [8]. These deleterious impacts on the V_{oc} and FF normally constrain the performance of single a-SiGe:H thin film solar cells. Consequently, numerous efforts have been reported where the focus was on formulating a method to raise the V_{oc} and FF while maintaining a high J_{sc} of the solar cells that uses the narrow-gap a-SiGe:H active layer [9, 10]. In spite of gaining significant improvement in V_{oc} and FF by different experimental models or designs [11, 12], the recombination loss mechanisms of the electric charge carriers are not very clear, although it is known that increased defects raise the recombination rate. As a result, a better understanding of the device operation may help identifying the pathways to further improve the device performance. One of the ways to understand the device performance is to investigate and compare performances of solar cells with constant low band gap and graded band gap active layer. Therefore, we investigated the recombination loss of photo-generated carriers in a-SiGe:H thin film solar cells.

2 Experiment

The amorphous silicon solar cells were fabricated with various active layers. The active layers had different Ge content. One type of solar cell (type-A) had purely a-SiGe:H as the active layer, that is of constant low band gap, and the other type of solar cell (type-B) had an active layer that was divided into four sub-layers, where the Ge content was different in each of the sub-layers. Device performances were compared by various measurements including the electrical bias dependent external quantum efficiency (EQE), variable illumination measurement (VIM) and dark current-voltage characteristics (DIV). The device parameters obtained from these measurements are collection losses (Q_{CL}), recombination losses (Q_{RL}), dynamic (shunt) resistance near short circuit condition (R_{sh}), reverse saturation current density (J_o), and diode quality factor (n). The a-SiGe:H thin film solar cells were fabricated by plasma enhanced chemical vapor deposition (PECVD) using a 13.56 MHz radio frequency power source in a multi-chamber system. The gas sources include silane (SiH_4), hydrogen (H_2) and germane (GeH_4) that were used as reactant gases for the intrinsic a-SiGe:H layer (i-layer). The composition gradient process of the entire i-layer of the type-B cells was implemented by controlling the GeH_4 to SiH_4 gas flow ratio during deposition of the active layers. The a-SiGe:H single-junction solar cells of type-A had a superstrate configuration as given follows: glass/ FTO/ AZO/ p-μc-SiO:H (10 nm)/ p-a-SiO:H (15 nm)/ i-a-Si:H buffer (15 nm)/ i-a-SiGe:H (300 nm)/ i-a-Si:H buffer (20 nm)/ n-μc-Si:H layer (40 nm)/ AZO/ Ag/ Al. Here, FTO is fluorine doped tin oxide, AZO is aluminum doped zinc oxide, i-a-SiGe:H is intrinsic a-SiGe:H, i-a-Si:H is intrinsic a-Si:H, p-μc-SiO:H is p-type high conductivity hydrogenated micro-crystalline silicon oxide, p-a-SiO:H is p-type hydrogenated amorphous silicon oxide and n-μc-Si:H is n-type hydrogenated micro-crystalline silicon layer. The investigated devices had the same physical structure except that there were differences in atomic composition of the active layers. We have observed that the p-type double layer, that was used in the device fabrication, is more beneficial than a single p-type layer. Details of the p-type double layer can be found in reference [2]. A thin protective layer of AZO over the FTO layer may be beneficial to protect the FTO electrode layer from possible hydrogen plasma damage, as well as texture induced surface defects [13].

The two types of solar cells that were investigated were of type-A and type-B. The solar cells of type-A were deposited with the following gas flow rates of the active layer; SiH_4 = 5 sccm, H_2 = 20 sccm, GeH_4 =1.1 sccm, while that of type-B had an active layer divided into four sub-layers of thickness 50 nm (front), 50 nm, 100 nm, 100 nm (back) all of which were prepared with constant gas flow rates of SiH_4 = 5 sccm, H_2 = 20 sccm, but the flow rates of the GeH_4 were changed as 1.1 sccm (front), 0.9 sccm, 0.7 sccm and 0.5 sccm (back) respectively. The cell of type–A or cell-A, had a constant low band gap (E_g) active layer with E_g = 1.58 eV, while that of type–B or cell-B, had an active layer with a positive gradient energy band gap E_g = 1.58, 1.61, 1.65, 1.68 eV [3]. The a-SiGe:H layer of the cell of type-A had Ge atomic content of 31.1 at.%, while that of the type-B had 31.1, 25.77, 20.48, 15.19 at.% respectively [3].

The cell parameters such as V_{oc}, J_{sc}, FF, and efficiency (E_{ff}) were calculated from J-V curve characteristic curves that were recorded under standard ambience and one sun-illumination. The VIM was examined under various illumination levels from 0.5 to 1 sun. The bias-voltage dependent external quantum efficiency was examined from −4 V to 0.8 V electrical bias for all the cells using the QEX7 model system of PV Measurement Inc. The film thickness was inferred from fitted spectroscopic ellipsometry data (V-VASE series, J. A. Woollam). The dark current voltage (DIV) characteristic curves were measured in dark condition by semiconductor test and analyzer (model EL420C).

3 Theoretical Model

The active layer (i-a-SiGe:H) of the cell of type-A or cell-A, had a constant low band gap, with high Ge content in the active layer, therefore its optical absorption and defect density is expected to be higher. Higher optical absorption can help in creating more electron-hole pairs in the active layer, but due to the higher defect density the electron-hole pairs will significantly be lost by recombination. Because of dependence of recombination on the generation, it can be expected that even though the a-SiGe:H based active layer can generate higher current density, that due to increased defect density the recombination loss will also be higher. It should also be noted that optical absorption follows the Beer-Lambert's exponential relation, therefore, towards the back of the cell where light intensity decreases, it may be necessary to reduce the recombination loss by defect reduction in this region. Here this is implemented in the form of forward grading of the band gap, that is implemented by reduction in Ge content of the active sub-layers towards the back of the cell and thereby raising the E_g of the sub-layers, which in turn reduces defect density of these sub-layers of the cell type-B.

The band gap grading can be intuitively seen in the band diagram as Fig. 1. The potential barriers at the p/i and i/n interfaces are expected to lower the hole and electron transport due to introduction of CG structure as in the cell of type B.

Figure 2 shows schematics of the composition gradient (CG) of active layer of cell type B, in comparison to cell A; the cell A was without the CG. The CG was implemented by changing the gas flow ratio, expressed as $[GeH_4]$ / $[GeH_4 + SiH_4]$. We call it a multistep grading as there are four divisions of the active layer with each division containing different atomic percent of Ge atoms.

Figure 3 shows the model of generation and recombination rates across the various layers of the cell. The electron-hole pair generation depends upon photon absorption. When photon energy is higher than the optical band gap of the material then each absorbed photon is expected

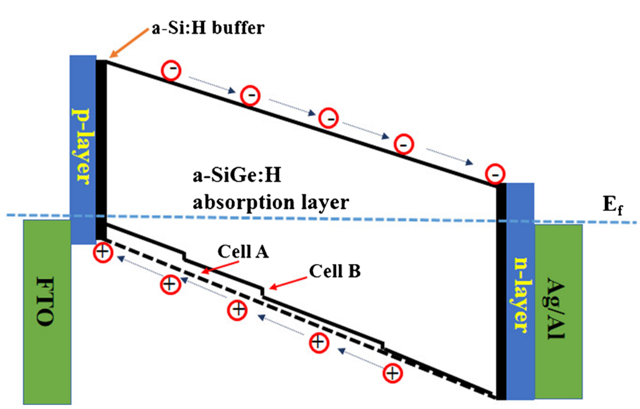

Fig. 1 The band diagram of cells with different composition gradient of intrinsic a-SiGe:H layer

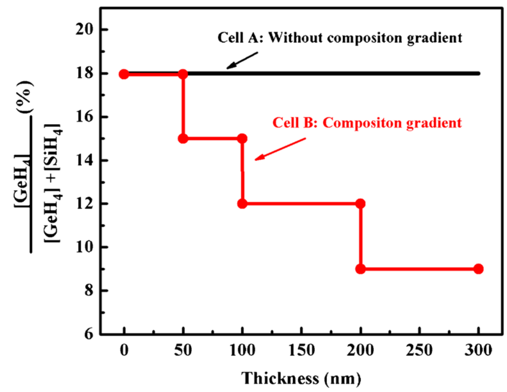

Fig. 2 Schematic diagram of a-SiGe:H solar cells with composition gradient of absorption layer

to create one electron hole pair. The Beer-Lambert exponential relation gives an expression for the optical absorption. When there are sub-band gap defects in a semiconductor, the photo-generated electron hole pairs face intense defect mediated recombination loss that is known as Shockley Read Hall recombination. In our investigation we estimated these generation and recombination losses across the solar cell by numerical simulation [14] and the results are given in Fig. 3. The results show that towards the front side of the cell the generation rates are the same for both the graded (type-B) and non-graded (type-A) cells. But afterwards, the generation rate of the cell type-A remains higher than that of the type-B. However, for the cells under maximum power point operation, there is a significant difference between the recombination rates of the cell type-A and type-B. In the front and first sub-layer of the active layer, where the composition of the cell type-A and type-B are the same, the

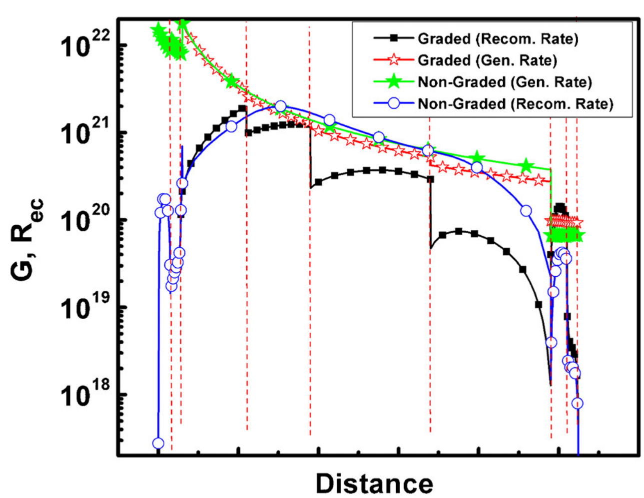

Fig. 3 Theoretical generation (G) and recombination (R) rates of carriers across the cell under AM1.5G illumination. The *vertical dotted lines* indicate interfaces with left-most line as interface between p- and buffer layer of the front side of the cell, on the right side it progresses towards the back of the cell

recombination rate of cell type-A remains lower than that of type-B, probably because of higher diffusive flow of photo-generated carriers from the interior towards the front side of the active layer of the cell. But afterwards, the recombination rate of the cell type-A remains significantly higher than that of the graded band gap cell type-B. The higher generation rate all across the active layer may help it to show higher J_{sc}. However, when the cell is operated at its maximum power point, the overall higher recombination loss of carriers may show as a lower fill factor and lower open circuit voltage.

4 Result and Discussion

4.1 Dark Current Characteristics

The dark current characteristics may give some insight into the quality of the solar cells [15, 16]. This dark characteristic curve was used to estimate the device parameters like reverse saturation current density (J_o) and ideality factor (n) from a plot of J versus (V-J*R_s), as shown in the inset of Fig. 4. Here R_s is defined as the series resistance in dark condition and is obtained from the intercept of the following expression: $dV/dJ = R_s + [(nkT/q) \times 1/J(V)]$, as shown in Fig. 4, here k, T, and q are the Boltzmann constant, measurement temperature and elementary charge of the electron respectively. The estimated diode parameters of the cells are summarized in Table 1. The carrier recombination in an amorphous silicon solar cell takes place both at the interface region, as well as in the bulk of the active layer. The change in the recombination loss can be detected by noticing the change in diode quality factor n and J_o [17]. Lower numerical value of the diode ideality factor indicates better electronic property of the diode. The best value of n is unity, however, the real cells show $n > 1$ indicating a dominant recombination in the bulk intrinsic layer [18, 19]. As seen in the Table 1, the value of n decreases from 1.8 to 1.7 along with decrease in J_o from 2×10^{-7} to 4.5×10^{-8} A/cm^2 for the cell with the CG. This indicates that the recombination in bulk of a-SiGe:H cells was reduced in the cell with the CG. Furthermore, the open circuit voltage can be expressed as $V_{oc} = (nkT/q) \times \ln(J_{sc}/J_o)$. It is clear that with the decrease in J_o of the cell type-B, its V_{oc} is expected to be higher as compared to the cell type-A. In particular, the considerable reduction in the recombination losses and the R_s due to the introduction of the CG in the active layer, might be a reason for the significant increase in FF of cell type-B, as shown in Table 1.

Table 1 Diode parameters under dark conditions of a-SiGe:H solar cells

Cell	Absorption Layer	J_o (A/cm^2)	n	R_s (Ω.cm^2)
A	Without Grading	2×10^{-7}	1.8	13.5
B	With Grading	4.5×10^{-8}	1.7	9.4

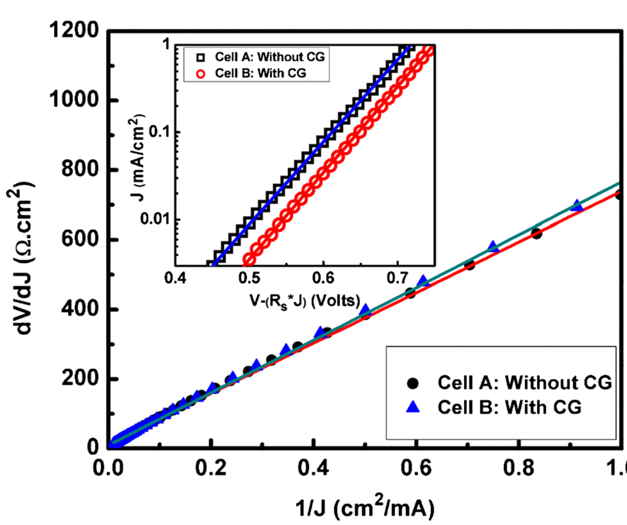

Fig. 4 Plot of dV/dJ as a function of 1/J for two cells from DIV characteristics. The intercept of the linear fitting line is the R_s value. The *inset* is plot of J as a function of (V-J*R) from which slope presents q/nkT and intercept is J_o

4.2 Illuminated Current Characteristics

The J-V characteristic curves of the cells under AM1.5G insolation is shown in Fig. 5, while the characteristic device parameters, V_{oc}, J_{sc}, FF and efficiency (E_{ff}), are presented in Table 2.

The intrinsic layer of the cell type-A has a lower optical gap than that of the cell B, so it has higher optical absorption and hence electron-hole pair generation rate (Fig. 3)

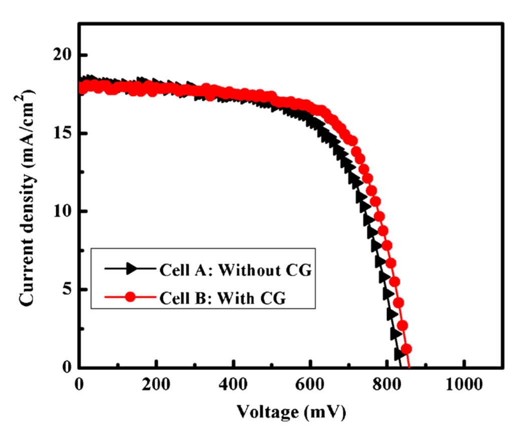

Fig. 5 J-V characteristic curves of cells under AM1.5G insolation

Table 2 Cell parameters under light conditions of a-SiGe:H solar cells

Cell	Absorption Layer	V_{oc} (V)	J_{sc} (mA/cm^2)	FF (%)	E_{ff} (%)	J_{oL} (A/cm^2)	n_L	R_{sL} (Ω.cm^2)
A	Without Grading	0.83	18.2	64	9.6	2.96 x 10^{-6}	3.73	0.18
B	With Grading	0.85	17.8	69	10.4	3.05 x 10^{-7}	3.06	0.94

The subscript "L" in the J_{oL}, n_L, R_{sL} indicates illumination condition

in comparison to the cell type-B, therefore the cell type-A shows a higher J_{sc}. However, its V_{oc} and FF remained lower than that of the cell type-B, that can be attributed to the enhanced recombination loss of electron-hole pairs in cell type-A due to the increased density of mid-gap defect states, Urbach energy at the band tail or micro-void types of defects [20, 21]. It has been reported that the redistribution of germanium atoms in the active layer can elevate the V_{oc} and the FF while this is somewhat detrimental to the J_{sc} [5, 6, 22]. As clearly seen in Fig. 5 and Table 2, the CG process in the cell type-B can raise the FF by 5% and V_{oc} by 20 mV, which leads to a high efficiency of 10.4%, although there was a decrease in J_{sc} by 0.4 mA. Several simulation and experimental works have been conducted by various research groups to interpret this increment [23–25]. One of the reasons is attributed to diminished carrier recombination loss in the active layer due to redistributions of Ge atoms in the a-SiGe:H active layer [5, 23]. We have already discussed a similar situation in Fig. 3.

4.3 Light Intensity Dependent Current Characteristics

In order to get an additional insight into the collection efficiency of the cells, the cell parameters were estimated from the current-voltage characteristics under variable illumination-intensity measurement (VIM) methods, as shown in Fig. 6. The Fig. 6a is for the cell type-A, while Fig. 6b is for cell type-B. Based on the VIM, the short circuit resistance (R_{sc}) value which is the negative reciprocal of the slope of the J-V curves at the short-circuit point (V=0) for different illumination levels, is shown in Fig. 7. Figure 7 shows the characteristic variation in R_{sc} with illumination intensity for cell type-A and B. It is generally understood that the cells with higher R_{sc} will show higher device efficiency.

The gross difference between the cell type-A and cell type-B is that the J_o of cell type-B are less than that of the cells type-A. The parameters that remain higher for cells type-A are the J_{oL}, n_L, R_{sL}, and $J_{sc,}$ where the subscript 'L' in J_{oL}, n_L, R_{sL}, indicates that these parameters were estimated from J-V characteristic curves of the solar cell under AM1.5G insolation [29]. These parameters are shown in Table 3. However, open circuit voltage, FF and efficiency of cells type-B are higher because of lower recombination loss in the active layer. This result further indicates that J_{sc} and J_0 increase with an increased level of illumination. The correlation is obvious as the carrier generation rate and hence the J_{sc} is proportional to the illumination intensity, furthermore, as recombination is also directly related to generation therefore J_o also increases, as it seems that the J_o is related to recombination.

4.4 External Quantum Efficiency

There are many different loss mechanisms that may exist in a solar cell. In a simple approach, these can be classified into three types as the recombination loss which adversely

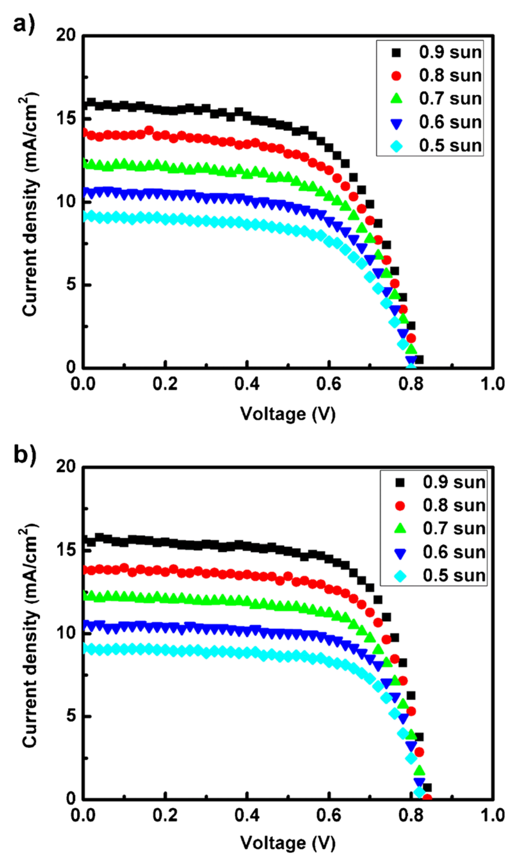

Fig. 6 **a** J-V curves of cell A under different light intensities. **b** J-V curves of cell B under different light intensities

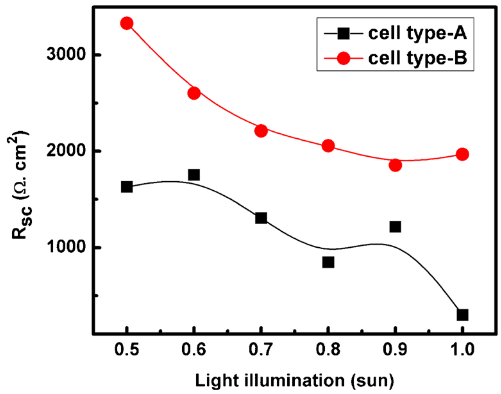

Fig. 7 Variation of R_{sc} with illumination intensity of the cells of type-A and B

affects the V_{oc}, the parasitic resistance losses which primarily limit the FF as well as V_{oc} and J_{sc}, and finally optical losses which have a strong impact on photo-generated carriers and J_{sc} [15]. In order to understand the reason, the carrier losses were estimated in the carrier collection process in an electrical bias dependent EQE measurement. The electrical bias used in the investigation were varied from −4 V to 0.8 V, and are shown in Fig. 8. It is well-known that in view of lower carrier lifetime in amorphous silicon thin film materials, the sufficient carrier collection primarily depends on the internal electric field which plays a primary role in driving and separating the carriers for collection to the electrodes [15]. In the reverse biased voltage dependent EQE, the externally applied electrical bias strengthens the electric field within the active layer or i-layer, resulting in better carrier collection and thus increased EQE [26]. If the reverse bias voltage is continuously elevated until the EQE reaches a saturation, at this point the internal electric field is attributed to being high enough to sufficiently drive all photo-generated carriers to collection and the EQE will reach a maximum where it is expected to minimize recombination losses [15, 26]. It can be seen in Fig. 8, that in the reverse bias range from −2V to −4V, the EQEs of cells change insignificantly or are nearly unchanged. It indicates that −4 V can be considered sufficient for saturation of carrier collection. Consequently, an EQE ratio as Q_{CL} = EQE (-4 V) / EQE (0 V) can be used to investigate the characteristic loss of the carriers. A large variation in the Q_{CL} spectra implies a large recombination loss in the collection process and vice versa. The results of the Q_{CL} spectra for the cells are shown in Fig. 9a. Comparing the Q_{CL} characteristics of the two cells indicates that the cell type-A had higher Q_{CL} than that of the cell type-B. It means electric field distribution and hence the carrier collection in cell type-B was better than that of cell type-A. In the short wavelength range (below 450 nm), both the cells perform close to each other but for the wavelength higher than this, the cell type-A showed a relatively poor performance. The active layer of the cell type-A had a larger Ge content and hence a lower optical gap. It is expected to have higher optical absorption as well as increased defect density. In the competition between the optical absorption related generation rate and the defect related recombination rate the larger defect density in the active layer of cell type-A resulted in poorer survival of the photo-generated carriers, as modeled in Fig. 3. Furthermore, the U-shape of the Q_{CL} curve indicates that in the middle of the spectral range (around 600 nm) both the cells showed a relatively better carrier collection. Beyond the 600 nm wavelength range both cells can have back-diffusion of electrons generated near the p/i interface to the p-layer due to the fact that this wavelength region is strongly absorbed in the vicinity of the p/i interface prior to the deeper impingement

Table 3 Solar cell parameters under VIM, n_L = 3.73 for cell A, and 3.06 for cell B

Cell	Sun	V_{oc} (mV)	J_{sc} (mA/cm^2)	FF (%)	E_{ff} (%)	J_{oL} (A/cm^2)	R_{sL} (Ω.cm^2)	R_{PL} (Ω.cm^2)
A	1	830	18.2	64	9.6	3.0×10^{-6}	0.18	720
	0.9	825	15.8	62	8.9	2.9×10^{-6}	–	573
	0.8	871	14.2	62	9.0	2.7×10^{-6}	2.2	1348
	0.7	811	12.3	63	9.0	2.5×10^{-6}	1.3	1314
	0.6	805	10.7	63	9.0	2.3×10^{-6}	1.2	1443
	0.5	800	9.15	64	9.4	2.3×10^{-6}	0.4	1274
B	1	850	17.8	69	10.4	3.1×10^{-7}	0.94	1200
	0.9	843	15.7	68	10.1	2.7×10^{-7}	0	995
	0.8	840	13.9	69	10.1	2.7×10^{-7}	0	1416
	0.7	835	12.2	68	10.0	2.6×10^{-7}	0	1299
	0.6	829	10.6	69	10.2	2.2×10^{-7}	0	1505
	0.5	824	9.1	70	10.6	1.3×10^{-7}	0	2157

Here 'R_{PL}' is the estimated shunt resistance from the illuminated J-V characteristic curves under 1 sun

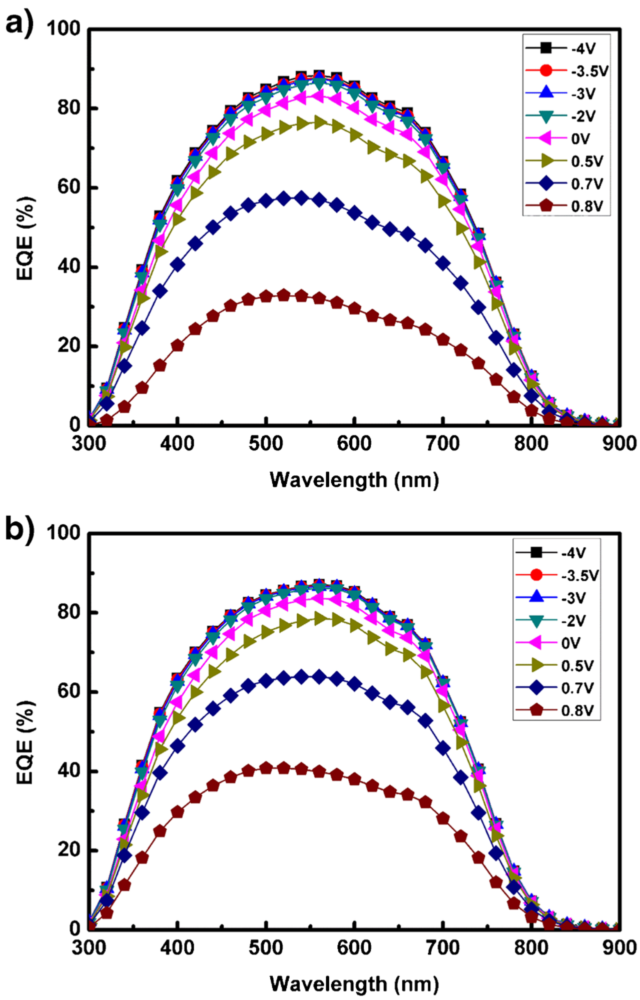

Fig. 8 **a** The voltage bias dependent EQE labeled with applied voltage of (**a**) cell A and (**b**) cell B. The *dash line* is a guide to the eyes

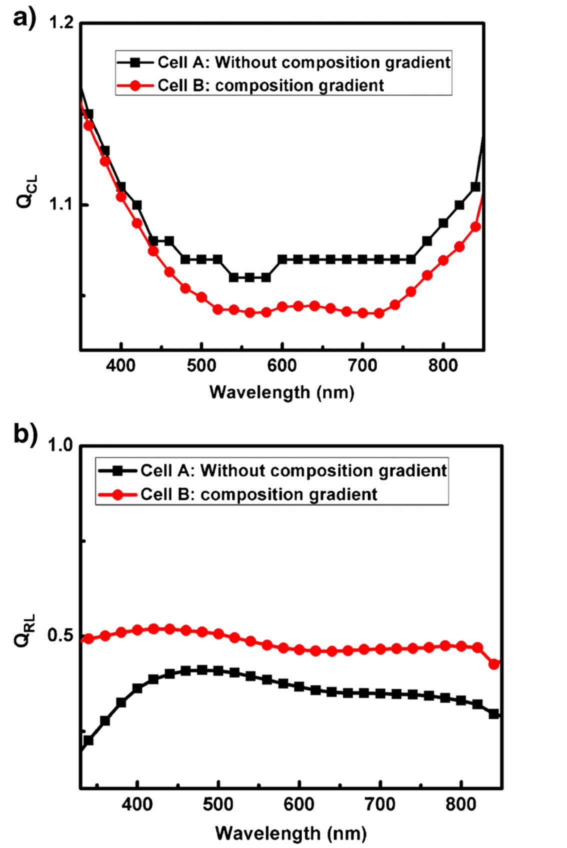

Fig. 9 The EQE ratio defined as (**a**) Q_{CL} = EQE (-4 V) / EQE (0 V) and (**b**) Q_{RL} = EQE (0.8 V) / EQE (0 V) of cells

of the photons [27]. Similarly, the longer wavelengths that are absorbed near the n/i interface face a similar problem with holes. The excess carrier loss at a longer wavelength radiation (longer than 450nm) can result from the recombination loss of the carriers in cell type-A. It should be noted from Fig. 9b that cell type-B leads to less photo-current loss, particularly in the wavelength region higher than 450 nm. In this range of light wavelength, based on light penetration, the photo-generated carriers may generate anywhere in the whole of the i-layer, especially in a location far from the p-layer [27]. Consequently, an efficient hole transport caused by the CG of cell B can help to improve the carrier collection in this range compared to the cell A [20].

The recombination losses in the active layer of the cells are further compared in the forward biased EQE measurement, examined from 0.5 V to 0.8 V. It is shown in Fig. 8. Due to the forward electrical bias an essential reduction in internal electric field takes place across the devices, leading to a decrease in EQE with increasing the bias [28]. As seen in Fig. 8, the EQE of both the cells decrease below the EQE (0 V) when the forward bias was increased from 0.5 V to 0.8 V. A lower reduction in the EQE is visible for the bias within 0.5 V – 0.7 V whereas a relatively large fall is visible for a bias over 0.7 V. As it is clear that the photo-carrier collection primarily depends on the internal electric field, and the forward bias reduces the internal electric field, so the change in the biased EQE is understandable. Here, the 0.8 V bias shows a very large reduction in the EQE, in this condition the carrier collection probably suffers from the high density of defects or traps which hinders their movement for the collection. For this purpose, a ratio defined by Q_{RL} = EQE (0.8 V) / EQE (0 V), can be used to differentiate the recombination losses in the active layers of the two types of cells. It is shown in Fig. 9b. The Q_{RL} of cell type-B is significantly higher than that of cell type-A, further indicating that the cell type-B is capable to perform better. This again shows that the CG process of cell type-B considerably reduces the recombination current in comparison to the cell type-A. Furthermore, it should be noticed that the Q_{RL} of cell type-B seems to remain very close to 0.5 in all wavelengths while for cell type-A, substantial losses are found at short wavelength below 450 nm. Based on these, it can be inferred that the recombination current is clearly dominated near the p/i and n/i interfaces of the cell type-A, which can be one of the reasons for low FF and V_{oc} in cell A [23].

In the early studies as reported in [20], the double profiling was an inverse profiling at the p/i interface that was combined with normal profiling along the rest of the intrinsic layer, improving cell performance than the other types of profiling. The later works were on various other types of band gap grading like U, V etc. In our work, the inverse profiling at the p/i interface is simply replaced by a thin a-Si:H buffer layer, which is similar to the inverse grading reported in [20]. Our work is also comparable to the U and V structure of the band gap profiling, although the p/i buffer is a thin layer with constant band gap. In order to compare our work with the inversely graded V and U type band structure, a major approximation can be made, then the energy band structure of the i-layer in our work can be compared as a common alternative to all these band structures. So in our cell, instead of inverse profiling, we have a thin step profiling that can also be compared to the left part of U and V type band structure. As we used a p-type silicon oxide layer in our device, so this step profiling or buffer layer seems to be more appropriate.

5 Conclusion

We investigated and compared performance of single junction solar cells due to a composition gradient of the a-SiGe:H active layer. The device efficiency improvement from 9.6% to 10.4% is due to the composition gradient. In comparison to the cell without the CG, the cell with the CG shows a reduced recombination loss of photo-generated carriers that is related to the high defect density of the absorption layer. The forward graded active layer in the cell resulted in an enhanced internal electric field and a more efficient collection of photo-generated carriers. Significantly reduced recombination losses in the cell with the CG is thought to be one of the main reasons for a higher V_{oc} and FF. Estimation of the losses in the carrier collection were conducted by electrical bias dependent EQE, VIM and DIV measurements from which the parameters characterizing the recombination losses within the absorption layer of the cells were Q_{CL}, Q_{RL}, n, J_o and R_s. Therefore the forward grading of the optical gap of the active layer of a solar cell is beneficial.

Acknowledgments This research was supported by the New & Renewable Energy Core Technology Program of the Korea Institute of Energy Technology Evaluation and Planning (KETEP), granted financial resource from the Ministry of Trade, Industry & Energy, Republic of Korea (No. 20163010012230).

References

1. Yan B, Yue G, Sivec L, Yang J, Guha S, Jiang C-S (2011) Innovative dual function nc-SiOx:H layer leading to a >16% efficient multi-junction thin-film silicon solar cell. Appl Phys Lett 99:113512
2. Cho J, Pham DP, Jung J, Shin C, Park J, Kim S, Tuan Le AH, Park H, Iftiquar SM, Yi J (2016) Improvement of hydrogenated amorphous silicon germanium thin film solar cells by different p-type contact layer. Mater Sci Semicond Process 41:480–484
3. Cho J, Iftiquar SM, Kim M, Park J, Jung J, Kim J, Yi J (2016) Hydrogenated amorphous silicon germanium active layer for top cell of a multi junction cell structure. J Nanosci Nanotechnol 16:4870–4874
4. Palinginis KC, Cohen JD, Yang JC, Guha S (2000) Defect bands in a-Si–Ge:H alloys with low Ge content. J Non-Crystal Solids 266–269(Part 2):665–669
5. Zimmer J, Stiebig H, Wagner H (1998) a-SiGe:H based solar cells with graded absorption layer. J Appl Phys 84:611–617
6. Jin-Won C, Jun Woong P, Yu Jin L, Seh-Won A, Heon-Min L, Park OO (2012) Graded layer modification for high efficiency hydrogenated amorphous silicon–germanium solar cells. Japan J Appl Phys 51:10NB16
7. Schüttauf J-W, Niesen B, Löfgren L, Bonnet-Eymard M, Stuckelberger, M, Hänni S, Boccard M, Bugnon G, Despeisse M, Haug F-J, Meillaud F, Ballif C (2015) Amorphous silicon–germanium for triple and quadruple junction thin-film silicon based solar cells. Solar Energy Mater Solar Cells 133:163–169
8. Lundszien D, Finger F, Wagner H (2002) A-Si:H buffer in a-SiGe:H solar cells. Solar Energy Mater Solar Cells 74:365–372
9. Lundszien D, Yong F, Finger F (2002) The influence of the optical band gap of buffer layers at the p/i- and i/n-side on the performance of amorphous silicon germanium solar cells. In: Photovoltaic specialists conference, 2002. Conference record of the twenty-ninth. IEEE, pp 1218–1221
10. Krajangsang T, Inthisang S, Dousse A, Moollakorn A, Hongsingthong, A, Kittisontirak S, Chinnavornrungsee P, Limmanee, A, Sritharathikhun J, Sriprapha K (2016) Band gap profiles of intrinsic amorphous silicon germanium films and their application to amorphous silicon germanium heterojunction solar cells. Opt Mater 51:245–249
11. Liu B, Bai L, Zhang X, Wei C, Huang Q, Sun J, Ren H, Hou G, Zhao Y (2015) Fill factor improvement in PIN type hydrogenated amorphous silicon germanium thin film solar cells: omnipotent N type μc-SiOx:H layer. Solar Energy Mater Solar Cells 140:450–456
12. Biron R, Pahud C, Haug F-J, Ballif C (2012) Origin of the V_{oc} enhancement with a p-doped nc-SiOx:H window layer in n-i-p solar cells. J Non-Crystal Solids 358:1958–1961
13. Park H, Iftiquar SM, Kim HW, Lee J, Le AHT, Yi J (2013) Diffused transmission and texture-induced defect with transparent conducting oxide front electrode of amorphous silicon solar cell. Semicond Sci Technol 28:115012

14. Stangl R, Haschke J, Leendertz C (2009) Numerical simulation of solar cells and solar cell characterization methods: the open-source on demand program Afors-het, Version 2.4 Rugescu RD (ed), Solarenergy, Intech, Croatia
15. Hegedus SS, Shafarman WN (2004) Thin-film solar cells: device measurements and analysis. Progress Photovolt Res Appl 12:155–176
16. Hegedus SS (1997) Current–voltage analysis of a-Si and a-SiGe solar cells including voltage-dependent photocurrent collection. Progress Photovolt Res Appl 5:151–168
17. Deng J, Wronski CR (2005) Carrier recombination and differential diode quality factors in the dark forward bias current-voltage characteristics of a-Si:H solar cells. J Appl Phys 98:024509
18. Deng J, Pearce JM, Koval RJ, Vlahos V, Collins RW, Wronski CR (2003) Absence of carrier recombination associated with the defect pool model in intrinsic amorphous silicon layers. Evidence from current–voltage characteristics on p–i–n and n–i–p solar cells. Appl Phys Lett 82:3023–3025
19. Fang J, Chen Z, Hou G, Wang F, Chen X, Wei C, Wang G, Sun J, Zhang D, Zhao Y, Zhang X (2015) High-quality hydrogenated intrinsic amorphous silicon oxide layers treated by H_2 plasma used as the p/i buffer layers in hydrogenated amorphous silicon solar cells. Solar Energy Mater Solar Cells 136:172–176
20. Guha S, Yang J, Pawlikiewicz A, Glatfelter T, Ross R, Ovshinsky, S R (1989) Band-gap profiling for improving the efficiency of amorphous silicon alloy solar cells. Appl Phys Lett 54:2330–2332
21. Jimenez Zambrano R, Rubinelli FA, Rath JK, Schropp REI (2002) Improvement in the spectral responseat long wavelength of a-SiGe:H solar cells by exponential band gap design of the i-layer. J Non-Crystal Solids 299–302(Part 2):1131–1135
22. Moon SY, You DJ, Lee SE, Lee H (2013) In-situ monitoring and control of hydrogenated amorphous silicon–germanium band-gap profiling during plasma deposition process. Curr Appl Phys 13:1502–1505
23. Zambrano RJ, Rubinelli FA, Arnoldbik WM, Rath JK, Schropp REI (2004) Computer-aided band gap engineering and experimental verification of amorphous silicon–germanium solar cells. Solar Energy Mater Solar Cells 81:73–86
24. Tang Z, Wang W, Wang D, Liu D, Liu Q, Yin M, He D (2010) The effect of Ar flow rate in the growth of SiGe:H thin films by PECVD. Appl Surf Sci 256:7032–7036
25. Pieters BE, Zeman M, van Swaaij RACMM, Metselaar WJ (2004) Optimization of a-SiGe:H solar cells with graded intrinsic layers using integrated optical and electrical modeling. Thin Solid Films 451–452:294–297
26. Abu-Ras D, Kirchartz T, Rau U (2011) Advanced characterization techniques for thin film solar cells. Wiley-VCH, Germany
27. Banerjee A, Xu X, Yang J, Guha S (1995) Carrier collection losses in amorphous silicon and amorphous silicon–germanium alloy solar cells. Appl Phys Lett 67:2975–2977
28. Chung Y-B, Lee D-K, Lim J-S, Hwang N-M (2011) Reduction of amorphous incubation layer by HCl addition during deposition of microcrystalline silicon by hot-wire chemical vapor deposition. Solar Energy Mater Solar Cells 95:211–214
29. Iftiquar SM, Yi J (2016) Low reverse saturation current density of amorphous silicon solar cell due to reduced thickness of active layer. J Electr Eng Technol 11:939–942